JACS
JOURNAL OF THE AMERICAN CHEMICAL SOCIETY

Article

XCage: A Tricyclic Octacationic Receptor for Perylene Diimide with Picomolar Affinity in Water

Wenqi Liu, Sharan Bobbala, Charlotte L. Stern, Jessica Hornick, Yugang Liu, Alan Enrique Enciso, Evan A. Scott, and J. Fraser Stoddart

J. Am. Chem. Soc., **Just Accepted Manuscript** • Publication Date (Web): 16 Jan 2020

Just Accepted

is published by the American Chemical Society. 1155 Sixteenth Street N.W., Washington, DC 20036

JACS JOURNAL OF THE AMERICAN CHEMICAL SOCIETY
Cite This: J. Am. Chem. Soc. XXXX, XXX, XXX−XXX
Article
pubs.acs.org/JACS

XCage: A Tricyclic Octacationic Receptor for Perylene Diimide with Picomolar Affinity in Water

Wenqi Liu,[1] Sharan Bobbala,[2] Charlotte L. Stern,[1] Jessica E. Hornick,[3,4] Yugang Liu,[2] Alan E. Enciso,[1] Evan A. Scott,[2] J. Fraser Stoddart*[1,5,6]

1. Department of Chemistry, 2145 Sheridan Road, Northwestern University, Evanston, IL 60208, USA

2. Department of Biomedical Engineering, 2145 Sheridan Road, Northwestern University, Evanston, IL 60208, USA

3. Chemistry of Life Processes Institute, Northwestern University, Evanston, Illinois 60208

4. Department of Molecular Biosciences, Northwestern University, Evanston, Illinois 60208, USA

5. Institute for Molecular Design and Synthesis, Tianjin University, Tianjin 300072, China

6. School of Chemistry, University of New South Wales, Sydney, NSW 2052, Australia

ABSTRACT

The rational design of wholly synthetic receptors that bind active substrates with ultrahigh affinities is a challenging goal, especially in water. Here, we report the synthesis of a tricyclic octacationic cyclophane, which exhibits complementary stereoelectronic binding towards a widely used fluorescent dye, perylene diimide, with picomolar affinity in water. The ultrahigh binding affinity is sustained by a large and rigid hydrophobic binding surface, which provides a highly favorable enthalpy and a slightly positive entropy of complexation. The receptor-substrate complex shows significant improvement in optical properties, including red-shifted absorption and emission, turn-on fluorescence, and efficient energy transfer. An unusual single-excitation, dual-emission, imaging study of living cells was performed by taking advantage of a large pseudo-Stokes shift, produced by the efficient energy transfer.

INTRODUCTION

High-affinity receptor-substrate recognition exists ubiquitously in biology where the concentrations of foreign substrates are maintained below a certain threshold by antibodies.[1] Billions of years of evolution have enabled nature to create these biological receptors with binding cavities that have high stereoelectronic complementarity towards their substrates down to the atomic level.[2] One of the grand challenges in supramolecular chemistry is to develop synthetic receptors with ultrahigh affinities, especially in water.[3–5] The majority of synthetic receptors described in the literature show[6] micromolar affinity or weaker binding. To date, examples of water compatible high-affinity receptors are rare and mainly limited to cucurbit[n]urils,[7–9] with a sparse distribution of them in pillararenes[10] and tetralactam macrocycles[11]. Exploring new synthetic receptor-substrate pairs with ultrahigh affinities in water will not only stand the chance of exposing fundamental insights into the origin of high-affinity interactions, but also deliver orthogonality towards the existing high-affinity receptor-substrate pairs with emergent properties[12] that meet the high demand in the fields of noncovalent click chemistry,[13] sensors,[14] advanced materials,[15–18] nanotechnology,[19] and biomedicine[20].

Towards this goal, Houk[6] has emphasized the importance of constructing large buried surface areas between receptors and substrates to achieve high-affinity binding. This principle is executed well by nature but proves challenging when it comes to the design of synthetic receptors capable of binding substrates in water.[12,13,21] Although extra binding surfaces are expected to deliver gains in binding enthalpy, restriction of conformational flexibility upon binding leads to losses of binding entropy, resulting in little or no gains in affinity – a concept known as enthalpy-entropy compensation.[22–24] Larger hydrophobic binding surfaces also cause poor water solubility, which

further hinders the structural design of synthetic receptors to achieve high-affinity binding in water.[25,26]

Recently, we have developed[27–29] a series of extended cationic cyclophanes characterized by large and rigid binding surfaces. These positively charged cyclophanes exhibit remarkable affinities towards polycyclic aromatic substrates with little conformational changes in organic solvents. The solubilities of these cyclophanes are highly dependent on their counterions. Generally speaking, the PF_6^- salts are soluble in MeCN whereas the Cl^- or $CF_3CO_2^-$ salts are soluble in water. The ability to manipulate large and rigid binding surfaces, without jeopardizing their solubilities, makes these cyclophanes ideal candidates for the design and synthesis of high affinity receptors in water.[30–34]

We began our investigation by using perylene diimide (**PDI**)-based dyes as the representative substrates, considering their superior photophysical properties and wide range of applications in materials science[35] and biotechnology[36]. Encapsulations of **PDI** dyes have been explored[37,38] using cucurbit[8]uril and also a tetracationic cyclophane, known[28] as **ExBox^{4+}**; significant improvements in photophysical properties of **PDI** dyes were observed in water. The affinity constants involving both these receptors remain around $10^5\ M^{-1}$ or lower in water. A closer inspection of these receptor-substrate pairs reveals that neither synthetic receptor is able to encapsulate completely the **PDI** molecule since the relatively large size of **PDI** imposes a particular challenge in identifying suitable receptors.

Herein, we report a new synthetic receptor that is tailored to provide a complementary stereoelectronic binding cavity for the **PDI** in water. We have chosen to name this tricyclic octacationic cyclophane receptor, **XCage^{8+},** in view of its X-shaped structure. **XCage^{8+}** features a roof-pillar-floor structure, where the roof and floor are each composed of a biphenyl unit, offering

a large and flat binding surface. Four *p*-xylylene units serve as pillars with the ideal lengths (7.0 Å) to support aromatic [π···π] stacking interactions (2 × 3.5 Å) with an included **PDI** molecule. The eight cationic pyridinium units provide both sufficient water solubility and complementary electronic binding sites for the four divergent carbonyl groups in the **PDI** molecule. The resulting **PDI** ⊂ **XCage**•$8CF_3CO_2$ complex, which exhibits picomolar binding affinity in water, is enthalpically driven along with a small favorable entropic component. Moreover, the strong binding is accompanied by a significant improvement in optical properties, including turn-on fluorescence, red-shifted absorption and emission, in addition to efficient energy transfer, which remains effective under cell-imaging conditions. The energy transfer results in a large pseudo-Stokes shift that is utilized in achieving a dual color imaging study of living cells using a single light excitation.

RESULTS AND DISCUSSION

Synthesis of XCage•$8CF_3CO_2$

XCage•$8CF_3CO_2$ was prepared (Figure 1a) in three steps from commercially available starting materials. The key building block **TB**•$4PF_6$ can be easily accessed by Suzuki coupling, followed by alkylation of pyridine units in 91% overall yield without the need of column chromatography. **XCage**•$8CF_3CO_2$ was obtained by a template-assisted synthesis with the help of TBAI as a catalyst.[39] Pyrene was used as a template and was subsequently removed[40] by continuous liquid-liquid extraction. The crude product was isolated by precipitation with TBACl and further purified by reverse-phase column chromatography. After anion exchange using TFA, $\mathbf{XCage}^{8+}$ was obtained as its $CF_3CO_2^-$ salt in 26% isolated yield. **XCage**•$8CF_3CO_2$ is highly soluble in water and MeOH, and slightly soluble in MeCN. It emits a blue fluorescence (10% quantum yield) in the

range of 350–550 nm in water.[41] The results of cyclic voltammetry experiments (Figure S26) reveal[42] a nonreversible redox process in Me_2SO.

X-Ray Crystallographic Analysis

Numerous attempts[43] to grow the single crystals of **XCage**$^{8+}$ with various counterions did not meet with success. Fortunately, a single crystal of **Perylene** ⊂ **XCage**•$8CF_3CO_2$ was obtained by slow vapor diffusion of *i*Pr_2O into a MeOH solution of **Perylene** ⊂ **XCage**•$8CF_3CO_2$. The solid-state structure of **XCage**•$8CF_3CO_2$ (Figure 1b) reveals that it has a box-like cavity with dimensions of 12.5 × 11.1 × 7.0 Å. The cavity volume (Figure S34) is estimated to be around 384 Å^3, which is comparable[44] with the cavity volume of cucurbit[8]uril. The roof and floor are parallel and supported by four *p*-xylylene pillars with an ideal distance (7.0 Å) for aromatic [π···π] stacking interactions. The large binding surface (Figure S33) of **XCage**$^{8+}$ covers 92% of the van der Waals surface of **Perylene**, which is sandwiched symmetrically between the roof and the floor. Moreover, the *p*-xylylene pillars provide further [CH···π] interactions with **Perylene** as revealed[45,46] by an independent gradient model (IGM) analysis (Figure S35).

A model compound **PDI1** (Figure 2) was synthesized in order to obtain the single-crystal superstructure of its 1:1 complex with **XCage**$^{8+}$. Like other **PDI** dyes, **PDI1** is poorly soluble in most solvents. In the presence of **XCage**•$8CF_3CO_2$, however, **PDI1** can be dissolved readily in solvents such as H_2O, MeOH, MeCN, DMF and Me_2SO. A single crystal of **PDI1** ⊂ **XCage**•$7PF_6$•OH was obtained by slow diffusion of Et_2O into a solution of **PDI1** ⊂ **XCage**•$8PF_6$ in MeCN. The solid-state superstructure (Figure 3d) reveals that each carbonyl group in **PDI1** is sandwiched between two pyridinium units with an average [C=O···N$^+$] distance of 4.4 Å, which

is the same [C=O···N^+] distance as that observed[47] in the diamantane ⊂ cucurbit[7]uril complex. There are in total eight [C=O···N^+] ion-dipole interactions within the complex, **PDI1** ⊂ **XCage^{8+}**. The core of **PDI1** is sandwiched between the two biphenyl units as a result of aromatic [π···π] stacking interactions and separated by a distance about 3.7 Å from the roof and the floor. A surface-area overlay analysis shows that 80% of the van der Waals surface of the **PDI1** core overlaps with **XCage^{8+}**. A similar analysis performed on a single crystal of a catenane shows[48] that only 40% of the PDI core overlaps with the ExBox^{4+} component.[49] Thus, **XCage^{8+}** provides twice the binding surface area compared to that of the ExBox^{4+} component in the catenane. IGM analysis reveals that **PDI** is enveloped by favorable van der Waals interactions with the biphenyl-containing roof and floor, as well as from the pyridinium and *p*-xylylene units. Moreover, the carbonyl groups on **PDI1** are involved in polar [C=O···HC] interactions with *p*-xylylene protons on **XCage^{8+}**. Interestingly, the planar surface of **PDI1** was found to be slightly twisted (12˚) in the bay region as a result of its aromatic [π···π] stacking interactions with the biphenyl-containing binding surfaces, which also exhibits a slightly twisted plane with a dihedral angle of 19˚. Such induced-fit binding is a well-established phenomenon[50] in receptor-substrate binding pairs in biological systems.

NMR Spectroscopy and Mass Spectrometry in Solution

In order to investigate the molecular recognition between **XCage**•8CF_3CO_2 and **PDI** in water, a water-soluble **PDI2** (Figure 2) flanked with two $mPEG_{2000}$ chains was synthesized.[51] A 1:1 mixture of **PDI2** and **XCage**•8CF_3CO_2 in D_2O produced **PDI2** ⊂ **XCage**•8CF_3CO_2 instantly in quantitative yield. Diagnostic changes in chemical shift, indicating complex formation, were revealed by comparison (Figure 4a) of the ^{1}H NMR spectra of **PDI2**, **PDI2** ⊂ **XCage**•8CF_3CO_2 and

XCage•$8CF_3O_2$. Large upfield shifts of the signal for protons A ($\Delta\delta = -0.41$ ppm) and protons B ($\Delta\delta = -0.61$ ppm) on **XCage**•$8CF_3CO_2$, together with a significant upfield shift of the signal for protons 2 ($\Delta\delta = -1.98$ ppm) on **PDI2**, indicate the presence of aromatic [$\pi\cdots\pi$] stacking interactions between **PDI2** and the biphenyl units. Meanwhile, large downfield shifts of the signal for protons D ($\Delta\delta = +0.29$ ppm) and protons F ($\Delta\delta = +0.37$ ppm) are a good indication of polar interactions between the imide carbonyl groups on **PDI2** and **XCage**•$8CF_3CO_2$ protons from both the pyridinium and xylylene moieties. A NOESY spectrum (Figure 4b) confirmed[52] the threaded structure with through-space corrections between protons 2 on **PDI2** and protons B, C and D on **XCage**•$8CF_3CO_2$. ESI-MS (Figure S25) confirmed the formation of **PDI2** ⊂ **XCage**•$8CF_3CO_2$ in water by revealing several peaks clustered around *m/z* 2000, 1500, 1200 and 1000, corresponding to different charged states of **PDI2** ⊂ **XCage**•$8CF_3CO_2$ along with the loss of between three and six $CF_3CO_2^-$ counterions. An analogous ^{1}H NMR spectroscopic experiment, designed to follow the formation of **PDI2** ⊂ **XCage**•$8CF_3CO_2$ in MeCN, is described in the Supporting Information.

Photophysical Properties

Encapsulation of **PDI2** by **XCage**•$8CF_3CO_2$ induces several distinctive changes in photophysical properties. In the UV-Vis spectra in MeCN, **PDI2** shows three sharp absorption peaks at 456, 484, and 520 nm, corresponding to the non-aggregated state of **PDI2**. This compound emits a bright yellow fluorescence with a 66% fluorescence quantum yield. In the presence of **XCage**•$8CF_3CO_2$, both the absorption and emission maxima of **PDI2** are red shifted (23-25 nm), whereas the fluorescence quantum yield remains unchanged. On the other hand, **PDI2** is highly aggregated in water, as indicated (Figure 5a) by the broad absorption peaks[53] and a low fluorescence quantum yield (4%).[54] Upon the addition of one molar equivalent of **XCage**•$8CF_3CO_2$, the color of the **PDI2**

solution changes instantly from dark red to bright orange; three distinctive absorption peaks at 472, 504, and 542 nm, the characteristic signature of monomeric **PDI** in solution, were observed. Meanwhile, the fluorescence quantum yield of **PDI2 ⊂ XCage•**$8CF_3CO_2$ in water increases up to 63%, which is close to the brightness of the complex in MeCN. Furthermore, the excitation and emission maxima of **PDI2 ⊂ XCage•**$8CF_3CO_2$ are red shifted (9–15 nm), and its fluorescence lifetime increases from 4.7 to 7.3 ns when compared with **PDI2**. Notably, the fluorescence of **PDI2 ⊂ XCage•**$8CF_3CO_2$ remains bright, even at high concentrations (>1 mM) in water, i.e., the condensed charges on **PDI2 ⊂ XCage•**$8CF_3CO_2$ prevent it from aggregating.

There is an efficient energy transfer from **XCage•**$8CF_3CO_2$ to **PDI2** in both MeCN and H_2O. In the excitation spectrum of **PDI2 ⊂ XCage•**$8CF_3CO_2$, we observed a strong excitation peak around 300 nm, where **XCage•**$8CF_3CO_2$ absorbs light. Remarkably, in MeCN, the fluorescence intensity of **PDI2 ⊂ XCage•**$8CF_3CO_2$, as a result of energy transfer, is 150% higher than that of the complex under direct excitation at 542 nm, suggesting a superior antenna effect. In water, the energy transfer process (Figure 5d) produces 86% of its original fluorescence intensity. By comparing the fluorescent emission of **XCage•**$8CF_3CO_2$ and **PDI2 ⊂ XCage•**$8CF_3CO_2$ at 350–525 nm, the energy transfer efficiencies are determined to be quantitative in MeCN and 90% in water.

Binding Kinetics and Thermodynamics

The changes in optical properties induced on **PDI2 ⊂ XCage•**$8CF_3CO_2$ complex formation enable a facile tracking of the recognition process. The kinetics of threading **PDI2** into **XCage•**$8CF_3CO_2$ in water was tracked by turn-on fluorescence as a function of time. The kinetic profile was fitted to a second order kinetic model and revealed $k_{on} = (4.8 \pm 1.1) \times 10^5\ M^{-1}s^{-1}$. The half-life at 0.1 μM was calculated to be 21 s. Such rapid complex formation of **PDI2 ⊂ XCage•**$8CF_3CO_2$ in water is

remarkable when one considers the threading process that involves the chain end of $mPEG_{2000}$ polymer finding a "correct" cavity entrance and then exiting at the right opening of the tricyclic cage. This observation agrees with the reported literature[55–57] that threading a PEG polymer through a macrocycle is rapid in water.

The binding constants (Table 1) were determined by fluorescence titration and isothermal titration calorimetry (ITC). Displacement titration experiments monitored by fluorescence[58] were performed in order to determine the high binding affinity between **PDI2** and **XCage•**$8CF_3CO_2$. In MeCN, binding of **XCage•**$8CF_3CO_2$ was tested first of all using **Perylene** as a substrate. Its binding constant was found to be in the order of 10^6 M^{-1}, which is similar in magnitude to that of **ExCage^{6+}•**$6PF_6$ and about 86 times higher than that of **ExBox^{4+}•**$4PF_6$.[28,29] Next, we performed a competitive experiment, starting with a solution of **XCage•**$8CF_3CO_2$ and 50 molar equivalents of **Perylene**. **PDI2** was titrated into the MeCN solution to displace **Perylene** from the cavity. The displacement titration was monitored by turn-on fluorescence and yielded a binding constant in the vicinity of 10^9 M^{-1}. The binding affinity between **XCage•**$8CF_3CO_2$ and **PDI2** in MeCN is too high to be evaluated by ITC, and only the binding enthalpy could be extracted from the isotherm. The Gibbs free energy was estimated from fluorescent titrations which also provide a $T\Delta S$ value. The formation of **PDI2** ⊂ **XCage•**$8CF_3CO_2$ in MeCN is mainly driven by favorable enthalpy with a small contribution from positive entropy. Compared with the binding of **Perylene** towards **XCage•**$8CF_3CO_2$, **PDI2** shows a similar positive ΔS and also enjoys a more negative ΔH, which originates from the additional [C=O···N^+] ion-dipole interactions.

In order to evaluate the affinity between **XCage•**$8CF_3CO_2$ and **PDI2** in water, we selected **Caffeine** as a competitor, considering its good solubility and structural similarity to **PDI**. The binding constants determined from both the fluorescence titration and ITC yielded similar results

that are in the order of 10^5 M^{-1}. The binding constant between **PDI2** and **XCage•**$8CF_3CO_2$ in water was subsequently measured in the presence of 1000 molar equivalents of **Caffeine**. As evaluated by the fluorescence titration, the binding constant between **PDI2** and **XCage•**$8CF_3CO_2$ was determined to be 7.7×10^{10} M^{-1}, i.e., K_d = 13 pM. The formation of **PDI2** ⊂ **XCage•**$8CF_3CO_2$ in water is enthalpically driven with a small favorable entropic component. The binding enthalpy observed in water is 4 kcal mol^{-1} higher when compared with that in MeCN, suggesting that the release of high energy water molecules provides[59] an extra contribution to the stability of **PDI2** ⊂ **XCage•**$8CF_3CO_2$ in addition to the large area [π-π] stacking and ion-dipole interactions. The small favorable entropy benefits[60] from the release of water into the bulk and the structural rigidity of both **XCage•**$8CF_3CO_2$ and **PDI2**.

In order to illustrate the effect of the extended receptor surface on the affinity enhancement, we investigated the binding thermodynamics of **ExBox•**4Cl — a structure analogue of **XCage•**$8CF_3CO_2$ — towards **PDI2** in water. **ExBox•**4Cl shows (Figure S48) a binding affinity of 2.0×10^6 M^{-1} and a binding enthalpy of –7.4 kcal mol^{-1}. Compared with **ExBox•**4Cl, **XCage•**$8CF_3CO_2$ enhances the binding affinity by a factor of 38,000 and provides twice amount of binding enthalpy. This observation is in line with the results of surface area overlap analysis, which reveals that **XCage**$^{8+}$ provides twice the binding surface area towards the **PDI** binding core compared to that of **ExBox**$^{4+}$. The extended binding surface results in significant gains in binding enthalpy ($\Delta\Delta H$ = –6.7 kcal mol^{-1}), while the loss of binding entropy ($T\Delta\Delta S$ = –0.5 kcal mol^{-1}) is trivial, leading to an obvious deviation[23] from the enthalpy-entropy compensation plots for cyclodextrin-guest complexation (Figure S53) and significantly enhanced affinity. These results prove that cationic cyclophanes with large and rigid binding surface are promising candidates to achieve high binding affinities in water.

Fluorescence Imaging Studies

The potential application of these emergent properties was illustrated by fluorescence imaging and flow cytometry studies with MCF-7 cells, i.e., a human breast adenocarcinoma cell line. **PDI2** ⊂ **XCage•**$8CF_3CO_2$ is non-toxic to MCF-7 cells and shows >95% cell viability at all concentrations tested (2.5–50 μM) (Figure S54). Live-cell confocal microscopic images of MCF-7 cells were collected after incubation with 10 μM **PDI2** or **PDI2** ⊂ **XCage•**$8CF_3CO_2$ for 6 h. Brightfield-merged images show (Figure 6a) no fluorescence after treatment with **PDI2** and a strong fluorescence signal after **PDI2** ⊂ **XCage•**$8CF_3CO_2$ treatment. The punctate signal of **PDI2** ⊂ **XCage•**$8CF_3CO_2$ co-localizes with the lysotracker signal (Figure S58), indicating the lysosomal localization of **PDI2** ⊂ **XCage•**$8CF_3CO_2$ inside the cells. The concentration-dependent uptake, observed by confocal microscopic analysis and flow cytometry studies, shows (Figure 6b and Figure S57) that the **PDI2** ⊂ **XCage•**$8CF_3CO_2$ could be detected inside MCF-7 cells at incubation concentrations as low as 0.1 μM. These results confirmed the superior fluorescence properties and high stability of **PDI2** ⊂ **XCage•**$8CF_3CO_2$ complex, even at low concentrations under cell-imaging conditions.

PDI2 ⊂ **XCage•**$8CF_3CO_2$ produces (Figure 5d) a similar fluorescence intensity as a result of efficient energy transfer when compared with the fluorescence by a direct excitation at 540 nm. Meanwhile, such an energy transfer process endows[61] the complex with a large pseudo-Stokes shift (239 nm). The bright fluorescence and large pseudo-Stokes shift are highly desirable for dual color imaging investigations[62] where a single light excitation can be used to excite two fluorophores that emit simultaneously in different wavelength regions. For this purpose, we first of all tested the effectiveness of cell imaging using energy transfer. MCF-7 cells were incubated with 20 μM **PDI2** ⊂ **XCage•**$8CF_3CO_2$ for 6 h and the live-cell fluorescence imaging was

performed by widefield microscopy. When **PDI2** ⊂ **XCage**•$8CF_3CO_2$ treated cells were excited using a DAPI excitation filter (ex: 381–399 nm), a bright fluorescence signal was detected (Figure 6c) with a TRITC emission filter (em: 571–617 nm). As a control, 20 μM **PDI2** treated cells did not show any fluorescence signal. Next, we tested the dual-color imaging, following incubation of MCF-7 cells with **PDI2** ⊂ **XCage**•$8CF_3CO_2$ and Hoechst 33342 stain (Hoechst), a widely used nucleus stain with excitation and emission peaks at 350 and 461 nm, respectively. The micrograph (Figure 6d) was obtained with a single DAPI excitation filter (ex: 381–399 nm) and two emission filters: DAPI (em: 411–459 nm) for Hoechst, and TRITC (em: 571–617 nm) for **PDI2** ⊂ **XCage**•$8CF_3CO_2$. The Hoechst stain was localized in the nucleus and visualized as a blue color. Meanwhile, **PDI2** ⊂ **XCage**•$8CF_3CO_2$ was visualized as the red punctate signals. These results demonstrate that the large pseudo-Stokes shift produced by efficient energy transfer can be utilized to achieve two-color channels imaging by a single light excitation, a procedure which has been explored previously with mutated fluorescent proteins[62] and synthetic dyes[63] that have large Stokes shifts. This property is highly desirable for the simultaneous study of two biological processes with advanced microscopic techniques, such as dual-color, single-laser fluorescence, cross-correlation spectroscopy[64] and multicolor stimulated emission depletion microscopy[65,66].

CONCLUSIONS

An octacationic tricyclic cyclophane **XCage**•$8CF_3CO_2$ has been designed and synthesized. **XCage**$^{8+}$ shows high complementary stereoelectronic binding towards **PDI** in water with picomolar affinity. The ultrahigh affinity of the complex is sustained by a blend of the hydrophobic effect as well as aromatic [π···π] stacking and ion-dipole interactions. This investigation proves that cationic cyclophanes with large and rigid surfaces are promising receptors for achieving high

binding affinities in water. Meanwhile, the strong-affinity binding pair reported here offers an orthogonality to existed high-affinity binding pairs that can be used in noncovalent click chemistry.[13]

The encapsulated **PDI** dye results in improved optical properties, increased solubility and efficient energy transfer. The potential application of these emergent properties was demonstrated by a single-excitation dual-emission imaging of living cells with **PDI2** ⊂ **XCage•**$8CF_3CO_2$ and Hoechst stain. While this research illustrates the bioimaging application of **PDI2** ⊂ **XCage•**$8CF_3CO_2$, it is worth emphasizing that there is a multitude of applications of **PDI** in various other scientific fields as well. The high affinity and exceptional optical properties of **PDI2** ⊂ **XCage•**$8CF_3CO_2$ provide a new starting point for the manipulation of **PDI** dyes with an eye to a wide range of applications in the fields of single-molecule electronics,[67–69] photonic device,[70] materials science,[35] and molecular biology.[36]

EXPERIMENTAL SECTION

Synthesis of XCage•$8CF_3CO_2$

A solution composed of **TPBP** (120 mg, 0.26 mmol), pyrene (315 mg, 1.60 mmol) and tetrabutylammonium iodide (20 mg, 0.05 mmol) in $CHCl_3$ (20 mL) was added to a solution of **TB•**$4PF_6$ (450 mg, 0.26 mmol) in MeCN (250 mL). The reaction mixture was heated at 85 ˚C for 3 days. After cooling to room temperature, tetrabutylammonium chloride (500 mg, 1.8 mmol) and $CHCl_3$ (300 mL) were added to the reaction mixture, the yellow precipitate was isolated by filtration and then dispersed in MeOH (100 mL). Celite (5g) and TFA (2 mL) were added, and the solvent was removed by vacuum. The remaining solid was loaded onto Combiflash flash

chromatography system and purified by reverse C_{18} columns using 0–25% MeCN/H_2O with 0.1% TFA as additive. Fractions containing the product were combined and MeCN was removed by vacuum. The remaining aqueous solution was extracted by continuous liquid-liquid extraction for 48 h until the yellow solution became colorless. Water was removed and the residue was further purified by reverse C_{18} chromatography using 0–15% MeCN/H_2O with 0.1% TFA as additive to obtain **XCage**•$8CF_3CO_2$ as a white solid (150 mg, 26% yield). ^{1}H NMR (500 MHz, CD_3OD) δ 9.15 – 9.09 (m, 16H), 8.81 (t, *J* = 2.0 Hz, 8H), 8.66 – 8.61 (m, 16H), 8.56 (q, *J* = 1.4 Hz, 4H), 7.75 (d, *J* = 2.5 Hz, 16H), 6.00 – 5.83 (m, 16H). ^{13}C NMR (125 MHz, CD_3OD) δ 159.9, 159.6, 154.5, 144.1, 138.9, 136.4, 135.3, 130.2, 128.6, 127.5, 125.5, 117.1, 114.8, 63.4. HRMS-ESI (m/z) for **XCage•8CF_3CO_2**: Calcd for $C_{108}H_{76}F_{18}N_8O_{12}^{2+}$: *m/z* = 1009.7659 $[M–2CF_3CO_2]^{2+}$; found 1009.7688 $[M–2CF_3CO_2]^{2+}$.

ASSOCIATED CONTENT

Supporting Information

The Supporting Information is available free of charge at https://pubs.acs.org/doi/

Chemical synthesis and characterization, mass spectral data, NMR spectra, X-ray crystal data, computational analysis, photophysical data, binding studies, and cell imaging data (PDF)

Crystallographic data for **TPBP** (CIF)

Crystallographic data for **Perylene ⊂ XCage**•$8CF_3CO_2$ (CIF)

Crystallographic data for **PDI1 ⊂ XCage**•$7PF_6$•OH (CIF)

Crystallographic data for **PDI1** (CIF)

AUTHOR INFORMATION

Corresponding Author

***** stoddart@northwestern.edu

ORCID

Wenqi Liu: 0000-0001-6408-0204

Sharan Bobbala: 0000-0002-0740-330X

Jessica E. Hornick: 0000-0002-2180-5399

Evan A. Scott: 0000-0002-8945-2892

J. Fraser Stoddart: 0000-0003-3161-3697

Notes

The authors declare no competing financial interest

ACKNOWLEDGEMENTS

The authors thank Professor Bradley D. Smith and Professor Douglas Philp for their insightful comments and suggestions on the manuscript. The authors also thank Dr. Margaret Schott for helping to polish the language in the manuscript. This research is part of the Joint Center of Excellence in Integrated Nano-Systems (JCIN) at King Abdulaziz City for Science and Technology (KACST) and Northwestern University (NU). The authors would like to thank both KACST and NU for their continued support of this research.

REFERENCES

(1) Szwajkajzer, D.; Carey, J. Molecular and Biological Constraints on Ligand-Binding Affinity and Specificity. *Biopolymers* **1997**, *44*, 181–198.

(2) Persch, E.; Dumele, O.; Diederich, F. Molecular Recognition in Chemical and Biological Systems. *Angew. Chem. Int. Ed.* **2015**, *54*, 3290–3327.

(3) Cremer, P. S.; Flood, A. H.; Gibb, B. C.; Mobley, D. L. Collaborative Routes to Clarifying The Murky Waters of Aqueous Supramolecular Chemistry. *Nat. Chem.* **2017**, *10*, 8–16.

(4) Liu, Y.; Zhao, W.; Chen, C.-H.; Flood, A. H. Chloride Capture Using a C-H Hydrogen Bonding Cage. *Science.* **2019**, *365*, 159–161.

(5) Tromans, R. A.; Carter, T. S.; Chabanne, L.; Crump, M. P.; Li, H.; Matlock, J. V.; Orchard, M. G.; Davis, A. P. A Biomimetic Receptor for Glucose. *Nat. Chem.* **2019**, *11*, 52–56.

(6) Houk, K. N.; Leach, A. G.; Kim, S. P.; Zhang, X. Binding Affinities of Host–Guest, Protein–Ligand, and Protein–Transition-state Complexes. *Angew. Chem. Int. Ed.* **2003**, *42*, 4872–4897.

(7) Shetty, D.; Khedkar, J. K.; Park, K. M.; Kim, K. Can We Beat The Biotin–Avidin Pair?: Cucurbit[7]uril-Based Ultrahigh Affinity Host–Guest Complexes and Their Applications. *Chem. Soc. Rev.* **2015**, *44*, 8747–8761.

(8) Assaf, K. I.; Nau, W. M. Cucurbiturils: From Synthesis to High-Affinity Binding and Catalysis. *Chem. Soc. Rev.* **2015**, *44*, 394–418.

(9) Barrow, S. J.; Kasera, S.; Rowland, M. J.; Del Barrio, J.; Scherman, O. A. Cucurbituril-Based Molecular Recognition. *Chem. Rev.* **2015**, *115*, 12320–12406.

(10) Ogoshi, T.; Yamagishi, T. A.; Nakamoto, Y. Pillar-Shaped Macrocyclic Hosts Pillar[n]arenes: New Key Players for Supramolecular Chemistry. *Chem.Rev* **2016**, *116*, 7937–8002.

(11) Li, D.-H.; Smith, B. D. Molecular Recognition Using Tetralactam Macrocycles with Parallel Aromatic Sidewalls. *Beilstein J. Org. Chem.* **2019**, *15*, 1086–1095.

(12) Liu, W.; Samanta, S. K.; Smith, B. D.; Isaacs, L. Synthetic Mimics of Biotin/(Strept)Avidin. *Chem. Soc. Rev.* **2017**, *46*, 2391–2403.

(13) Schreiber, C. L.; Smith, B. D. Molecular Conjugation Using Non-Covalent Click Chemistry. *Nat. Rev. Chem.* **2019**, *3*, 393–400.

(14) Mako, T. L.; Racicot, J. M.; Levine, M. Supramolecular Luminescent Sensors. *Chem. Rev.* **2019**, *119*, 322–477.

(15) Heinzmann, C.; Weder, C.; de Espinosa, L. M. Supramolecular Polymer Adhesives: Advanced Materials Inspired by Nature. *Chem. Soc. Rev.* **2015**, *342*, 342–358.

(16) Wang, H.; Ji, X.; Li, Z.; Huang, F. Fluorescent Supramolecular Polymeric Materials. *Adv. Mater.* **2017**, *29*, 1606117.

(17) Ariga, K.; Li, J.; Fei, J.; Ji, Q.; Hill, J. P. Nanoarchitectonics for Dynamic Functional Materials from Atomic-/Molecular-Level Manipulation to Macroscopic Action. *Adv. Mater.* **2016**, *28*, 1251–1286.

(18) Pan, J.; Chen, W.; Ma, Y.; Pan, G. Molecularly Imprinted Polymers as Receptor Mimics for Selective Cell Recognition. *Chem. Soc. Rev.* **2018**, *47*, 5574–5587.

(19) Sarikaya, M.; Tamerler, C.; Jen, A. K.-Y.; Schulten, K.; Baneyx, F. Molecular Biomimetics: Nanotechnology through Biology. *Nat. Mater.* **2003**, *2*, 577–585.

(20) Webber, M. J.; Langer, R. Drug Delivery by Supramolecular Design. *Chem. Soc. Rev.* **2017**, *46*, 6600–6620.

(21) Murray, J.; Kim, K.; Ogoshi, T.; Yao, W.; Gibb, B. C. The Aqueous Supramolecular Chemistry of Cucurbit[n]urils, Pillar[n]Arenes and Deep-Cavity Cavitands. *Chem. Soc. Rev.* **2017**, *46*, 2479–2496.

(22) Chodera, J. D.; Mobley, D. L. Entropy-Enthalpy Compensation: Role and Ramifications in Biomolecular Ligand Recognition and Design. *Annu. Rev. Biophys.* **2013**, *42*, 121–142.

(23) Rekharsky, M. V; Mori, T.; Yang, C.; Ko, Y. H.; Selvapalam, N.; Kim, H.; Sobransingh, D.; Kaifer, A. E.; Liu, S.; Isaacs, L.; et al. A Synthetic Host-Guest System Achieves Avidin-Biotin Affinity by Overcoming Enthalpy-Entropy Compensation. *Proc. Natl. Acad. Sci. U. S. A.* **2007**, *104*, 20737–20742.

(24) Liu, W.; Johnson, A.; Smith, B. D. Guest Back-Folding: A Molecular Design Strategy That Produces a Deep-Red Fluorescent Host/Guest Pair with Picomolar Affinity in Water. *J. Am. Chem. Soc.* **2018**, *140*, 3361–3370.

(25) Spenst, P.; Würthner, F. A Perylene Bisimide Cyclophane as a “Turn-On” and “Turn-Off” Fluorescence Probe. *Angew. Chem. Int. Ed.* **2015**, *54*, 10165–10168.

(26) Sapotta, M.; Hofmann, A.; Bialas, D.; Würthner, F. A Water-Soluble Perylene Bisimide Cyclophane as A Molecular Probe for The Recognition of Aromatic Alkaloids. *Angew. Chem. Int. Ed.* **2019**, *58*, 3516–3520.

(27) Dale, E. J.; Vermeulen, N. A.; Juríček, M.; Barnes, J. C.; Young, R. M.; Wasielewski, M. R.; Stoddart, J. F. Supramolecular Explorations: Exhibiting The Extent of Extended Cationic Cyclophanes. *Acc. Chem. Res.* **2016**, *49*, 262–273.

(28) Barnes, J. C.; Juríček, M.; Strutt, N. L.; Frasconi, M.; Sampath, S.; Giesener, M. A.; McGrier, P. L.; Bruns, C. J.; Stern, C. L.; Sarjeant, A. A.; et al. ExBox: A Polycyclic Aromatic Hydrocarbon Scavenger. *J. Am. Chem. Soc.* **2013**, *135*, 183–192.

(29) Dale, E. J.; Vermeulen, N. A.; Thomas, A. A.; Barnes, J. C.; Juríček, M.; Blackburn, A. K.; Strutt, N. L.; Sarjeant, A. A.; Stern, C. L.; Denmark, S. E.; et al. ExCage. *J. Am. Chem. Soc.* **2014**, *136*, 10669–10682.

(30) Tsutsui, T.; Kusaba, S.; Yamashina, M.; Akita, M.; Yoshizawa, M. Open Versus Closed Polyaromatic Nanocavity: Enhanced Host Abilities toward Large Dyes and Pigments. *Chem. Eur. J* **2019**, *25*, 4320–4324.

(31) Yoshizawa, M.; Catti, L. Bent Anthracene Dimers as Versatile Building Blocks for Supramolecular Capsules. *Acc. Chem. Res.* **2019**, *52*, 2392–2404.

(32) Yamashina, M.; Tsutsui, T.; Sei, Y.; Akita, M.; Yoshizawa, M. A Polyaromatic Receptor with High Androgen Affinity. *Sci. Adv.* **2019**, *5*, 1–8.

(33) Jono, K.; Suzuki, A.; Akita, M.; Albrecht, K.; Yamamoto, K.; Yoshizawa, M. A Polyaromatic Molecular Clip That Enables the Binding of Planar, Tubular, and Dendritic Compounds. *Angew. Chem. Int. Ed.* **2017**, *56*, 3570–3574.

(34) Yamauchi, Y.; Yoshizawa, M.; Akita, M.; Fujita, M. Engineering Double to Quintuple Stacks of a Polarized Aromatic in Confined Cavities. *J. Am. Chem. Soc.* **2010**, *132*, 960–966.

(35) Würthner, F.; Saha-Möller, C. R.; Fimmel, B.; Ogi, S.; Leowanawat, P.; Schmidt, D. Perylene Bisimide Dye Assemblies as Archetype Functional Supramolecular Materials. *Chem. Rev.* **2016**, *116*, 962–1052.

(36) Sun, M.; Müllen, K.; Yin, M. Water-Soluble Perylenediimides: Design Concepts and Biological Applications. *Chem. Soc. Rev.* **2016**, *45*, 1513–1528.

(37) Ryan, S. T. J.; Del Barrio, J.; Ghosh, I.; Biedermann, F.; Lazar, A. I.; Lan, Y.; Coulston, R. J.; Nau, W. M.; Scherman, O. A. Efficient Host-Guest Energy Transfer in Polycationic Cyclophane-Perylene Diimide Complexes in Water. *J. Am. Chem. Soc.* **2014**, *136*, 9053–9060.

(38) Biedermann, F.; Elmalem, E.; Ghosh, I.; Nau, W. M.; Scherman, O. A. Strongly Fluorescent, Switchable Perylene Bis(Diimide) Host-Guest Complexes with Cucurbit[8]uril in Water. *Angew. Chem. Int. Ed.* **2012**, *51*, 7739–7743.

(39) Barnes, J. C.; Juríček, M.; Vermeulen, N. A.; Dale, E. J.; Stoddart, J. F. Synthesis of Ex^{n}Box Cyclophanes. *J. Org. Chem.* **2013**, *78*, 11962–11969.

(40) In the absence of template, no product could be isolated on account of the structural flexibilty of **TB**•4PF6. The presence of pyrene template helps preorganize and rigidify the precusor and faciliate **XCage**$^{8+}$ formation. Moreover, the template also helps visualize the formation of **XCage**$^{8+}$, which forms a yellow precipitate from the reaction mixture after its complexation with pyrene.

(41) The absolute fluorescent quantum yield of **XCage**•8CF_3CO_2 in water was measured using an integrating sphere detector.

(42) The nonreversible redox process of **XCage**•8CF_3CO_2 in Me_2SO is a result of the poor solubilites of the neutral species upon redution. After the first redox cycle, precipitations were observed on electrodes, and no redox signal could be further detected.

(43) Large (>100 μm in diameter) block-like crystals can be obtained by slow diffusion of Et_2O into a MeOH solution of **XCage•**$8CF_3CO_2$. These crystals showed poor X-ray diffraction, which prevented further structural determination.

(44) Nau, W. M.; Florea, M.; Assaf, K. I. Deep Inside Cucurbiturils: Physical Properties and Volumes of Their Inner Cavity Determine The Hydrophobic Driving Force for Host-Guest Complexation. *Isr. J. Chem.* **2011**, *51*, 559–577.

(45) Lefebvre, C.; Rubez, G.; Khartabil, H.; Boisson, J. C.; Contreras-García, J.; Hénon, E. Accurately Extracting The Signature of Intermolecular Interactions Present in The NCI Plot of The Reduced Density Gradient Versus Electron Density. *Phys. Chem. Chem. Phys.* **2017**, *19*, 17928–17936.

(46) Lu, T.; Chen, F. Multiwfn: A Multifunctional Wavefunction Analyzer. *J. Comput. Chem.* **2012**, *33*, 580–592.

(47) Cao, L.; Sekutor, M.; Zavalij, P. Y.; Mlinaric-Majerski, K.; Glaser, R.; Isaacs, L. Cucurbit[7]uril.Guest Pair with an Attomolar Dissociation Constant. *Angew. Chem., Int. Ed.* **2014**, *53*, 988–993.

(48) Ryan, S. T. J.; Young, R. M.; Henkelis, J. J.; Hafezi, N.; Vermeulen, N. A.; Hennig, A.; Dale, E. J.; Wu, Y.; Krzyaniak, M. D.; Fox, A.; et al. Energy and Electron Transfer Dynamics within a Series of Perylene Diimide/Cyclophane Systems. *J. Am. Chem. Soc.* **2015**, *137*, 15299–15307.

(49) A bolded descriptor denotes a compound, be it free or complexed, and an unbolded descriptor refers to either (i) a component within a compound or (ii) a component part of a mechanically interlocked molecule.

(50) Ringe, D.; Petsko, G. A. How Enzymes Work. *Science.* **2008**, *320*, 1428–1429.

(51) **PDI1** is polydispersed with an average molecular weight about 4000 according to electrospray ionization mass spectrometry.

(52) The NOESY spectrum was obtained using 0.2 s mixing time. The ^{1}H NMR spectrum of PEG chains were found to split into several peaks between 3.05 ppm and 4.20 ppm; these peaks also reveals through-space correlations with **XCage**$^{8+}$ in NOESY experiments.

(53) Heek, T.; Fasting, C.; Rest, C.; Zhang, X.; Würthner, F.; Haag, R. Highly Fluorescent Water-Soluble Polyglycerol-Dendronized Perylene Bisimide Dyes. *Chem. Commun.* **2010**, *46*, 1884–1886.

(54) The observed weak fluorescence of **PDI2** originates from residual monomeric species, judging from its excitation spectrum.

(55) Ishida, T.; Morisaki, Y.; Chujo, Y. Synthesis of Covalently Bonded Nanostructure from Two Porphyrin Molecular Wires Leading to a Molecular Tube. *Tetrahedron Lett.* **2006**, *47*, 5265–5268.

(56) Yamashina, M.; Kusaba, S.; Akita, M.; Kikuchi, T.; Yoshizawa, M. Cramming Versus Threading of Long Amphiphilic Oligomers into a Polyaromatic Capsule. *Nat. Commun.* **2018**, *9*, 3–9.

(57) Deutman, A. B. C.; Monnereau, C.; Elemans, J. a a W.; Ercolani, G.; Nolte, R. J. M.; Rowan, A. E. Mechanism of Threading a Polymer through a Macrocyclic Ring. *Science.* **2008**, *322*, 1668–1671.

(58) An effort to determine the binding constants between **XCage^{8+}** and **PDI2** using the displacement ITC method in both MeCN and water did not meet with success on account of the mutal aggregation among **XCage^{8+}**, competitors, **PDI2**, and their corresponding complexes.

(59) Biedermann, F.; Nau, W. M.; Schneider, H. J. The Hydrophobic Effect Revisited - Studies with Supramolecular Complexes Imply High-Energy Water as a Noncovalent Driving Force. *Angew. Chem. Int. Ed.* **2014**, *53*, 11158–11171.

(60) Gibb, B. C. Supramolecular Assembly and Binding in Aqueous Solution: Useful Tips Regarding The Hofmeister and Hydrophobic Effects. *Isr. J. Chem.* **2011**, *51*, 798–806.

(61) Fan, J.; Hu, M.; Zhan, P.; Peng, X. Energy Transfer Cassettes Based on Organic Fluorophores: Construction and Applications in Ratiometric Sensing. *Chem. Soc. Rev.* **2013**, *42*, 29–43.

(62) Chu, J.; Oh, Y.; Sens, A.; Ataie, N.; Dana, H.; Macklin, J. J.; Laviv, T.; Welf, E. S.; Dean, K. M.; Zhang, F.; et al. A Bright Cyan-Excitable Orange Fluorescent Protein Facilitates Dual-Emission Microscopy and Enhances Bioluminescence Imaging in Vivo. *Nat. Biotechnol.* **2016**, *34*, 760–767.

(63) Garwin, S. A.; Kelley, M. S. J.; Sue, A. C.; Que, E. L.; Schatz, G. C.; Woodruff, T. K.; O'Halloran, T. V. Interrogating Intracellular Zinc Chemistry with a Long Stokes Shift Zinc Probe ZincBY-4. *J. Am. Chem. Soc.* **2019**, *141*, 16696–16705.

(64) Kogure, T.; Karasawa, S.; Araki, T.; Saito, K.; Kinjo, M.; Miyawaki, A. A Fluorescent Variant of a Protein from The Stony Coral Montipora Facilitates Dual-Color Single-Laser Fluorescence Cross-Correlation Spectroscopy. *Nat. Biotechnol.* **2006**, *24*, 577–581.

(65) Butkevich, A. N.; Lukinavičius, G.; D'Este, E.; Hell, S. W. Cell-Permeant Large Stokes Shift Dyes for Transfection-Free Multicolor Nanoscopy. *J. Am. Chem. Soc.* **2017**, *139*, 12378–12381.

(66) Sednev, M. V.; Belov, V. N.; Hell, S. W. Fluorescent Dyes with Large Stokes Shifts for Super-Resolution Optical Microscopy of Biological Objects: A Review. *Methods Appl. Fluoresc.* **2015**, *3*, 042004.

(67) Weil, T.; Vosch, T.; Hofkens, J.; Peneva, K.; Müllen, K. The Rylene Colorant Family-Tailored Nanoemitters for Photonics Research and Applications. *Angew. Chem. Int. Ed.* **2010**, *49*, 9068–9093.

(68) Li, X.; Hihath, J.; Chen, F.; Masuda, T.; Zang, L.; Tao, N. Thermally Activated Electron Transport in Single Redox Molecules. *J. Am. Chem. Soc.* **2007**, *129*, 11535–11542.

(69) Xu, B.; Xiao, X.; Yang, X.; Zang, L.; Tao, N. Large Gate Modulation in The Current of a Room Temperature Single Molecule Transistor. *J. Am. Chem. Soc.* **2005**, *127*, 2386–2387.

(70) Xin, N.; Guan, J.; Zhou, C.; Chen, X.; Gu, C.; Li, Y.; Ratner, M. A.; Nitzan, A.; Stoddart, J. F.; Guo, X. Concepts in The Design and Engineering of Single-Molecule Electronic Devices. *Nat. Rev. Phys.* **2019**, *1*, 211–230.

Captions for Figures

Figure 1. (a) Synthesis of **XCage**•$8CF_3CO_2$. (b) Solid-state superstructures of **Perylene** ⊂ **XCage**$^{8+}$ obtained from single-crystal X-ray crystallography. Counterions and solvents are omitted for the sake of clarity

Figure 2. Substrates molecules evaluated in the present study. **Perylene** and **caffeine** are used as competitive substrates for displacement studies. **PDI2** has been modified with polydispersed PEG chains to enhance its solubility in water

Figure 3. (a) Plan and (b) side-on views of the solid-state superstructure of **PDI1** ⊂ **XCage**$^{8+}$ obtained from single-crystal X-ray crystallography. (c) Surface-area overlap analysis of **PDI1** ⊂ **XCage**$^{8+}$. Half of **XCage**$^{8+}$ is deleted for the sake of clarity. Green: roof or floor; yellow: pillar units; Red: total area of the **PDI** core; Dark red: overlapping area. (d) [$N^+\cdots O{=}C$] ion-dipole interaction distances in **PDI1** ⊂ **XCage**$^{8+}$. (e) Electrostatic potential map of the **PDI** core

Figure 4. (a) ^{1}H NMR (500 MHz, D_2O, 25 ˚C) spectra of **PDI2** (top), **PDI2** ⊂ **XCage**•$8CF_3CO_2$ (middle), and **XCage**•$8CF_3CO_2$ (bottom). (b) ^{1}H-^{1}H NOESY (500 MHz, D_2O, 25 ˚C) of **PDI2** ⊂ **XCage**•$8CF_3CO_2$. Protons labels are shown in Figure 1 and Figure 2. All samples were measured at 1.5 mM concentration

Figure 5. (a) Absorption and (b) emission (ex: 440 nm) spectra of **PDI2** (blue) and **PDI2** ⊂ **XCage**•$8CF_3CO_2$ (red) in water: inserts show aqueous solutions of **PDI2** (left) and **PDI2** ⊂ **XCage**•$8CF_3CO_2$ (right) under day light and UV light (ex: 365 nm). (c) Emission spectra (ex: 290 nm) of **PDI2** (blue) and **PDI2** ⊂ **XCage**•$8CF_3CO_2$ (red) in water. (d) Excitation spectra (em: 600 nm) of **PDI2** (blue) and **PDI2** ⊂ **XCage**•$8CF_3CO_2$ (red) in water

Figure 6. (a) Brightfield-merged micrograph of MCF-7 cells treated with **PDI2** and **PDI2** ⊂ **XCage**$^{8+}$. Images were obtained using a 514 nm confocal laser with an emission window in the range of 530–580 nm. Scale bar: 20 µm. (b) Concentration dependent uptake of **PDI2** ⊂ **XCage**$^{8+}$ by MCF-7 cells analyzed by flow cytometry (ex: 552 nm) in the PE-Cy5 channel (em: 656–684 nm); MFI represents mean fluorescence intensity. (c) Fluorescence micrograph of MCF-7 cells with **PDI2** and **PDI2** ⊂ **XCage**$^{8+}$. Images were obtained using a DAPI excitation filter (ex: 381–399 nm) and a TRITC emission filter (em: 571–617 nm). (d) Dual-color micrograph of MCF-7 cells with Hoechst and **PDI2** ⊂ **XCage**$^{8+}$. Images were obtained using a single DAPI excitation filter (ex: 381–399 nm) and two emission filters: DAPI emission filter (em: 411–459 nm) and TRITC emission filter (em: 571–617 nm). Scale bar: 25 µm

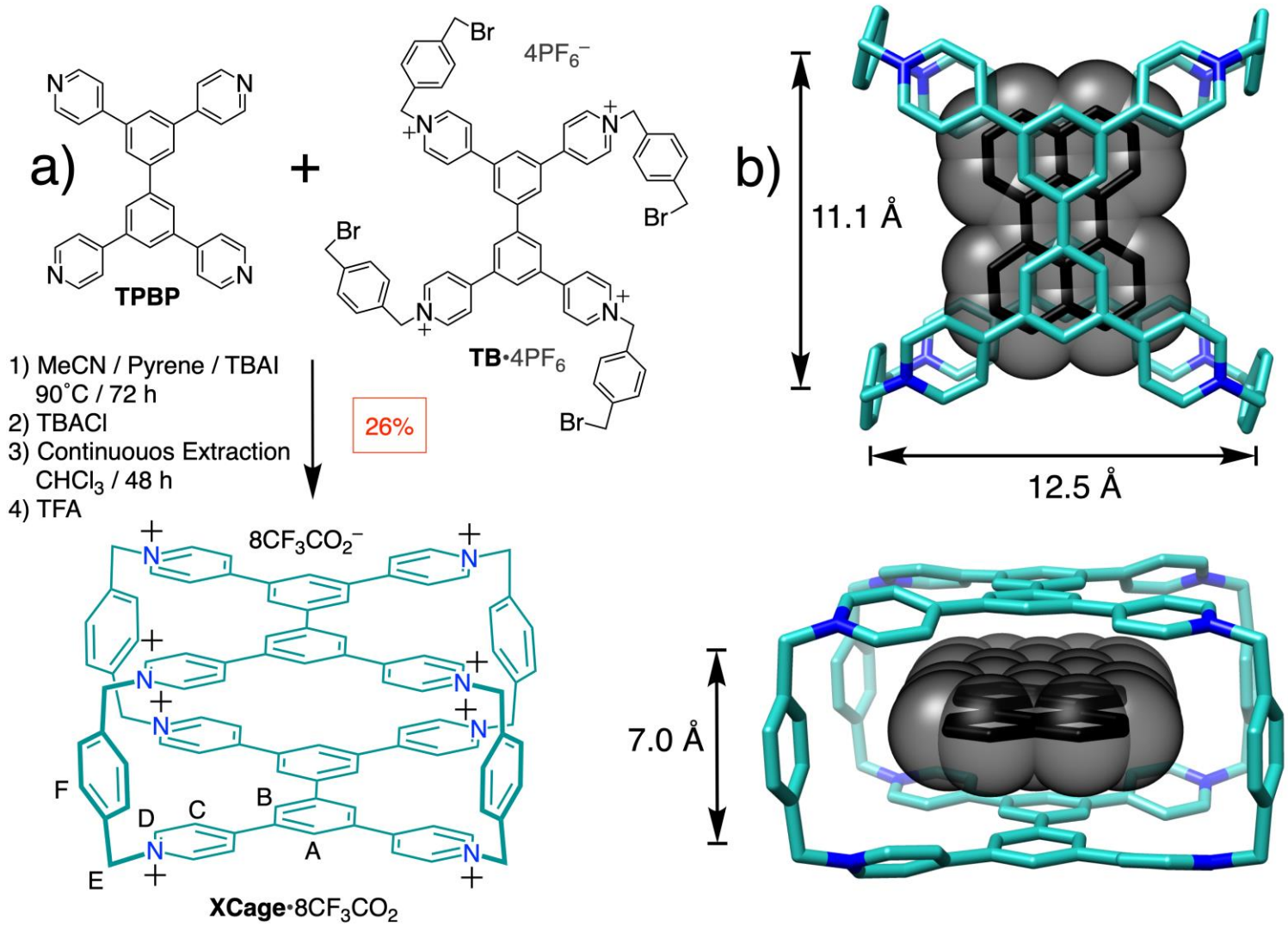
a)
TPBP
+
Br
4PF6−
Br
Br
Br
TB·4PF6
1) MeCN / Pyrene / TBAI
90˚C / 72 h
2) TBACl
3) Continuouos Extraction
CHCl3 / 48 h
4) TFA
26%
8CF3CO2−
F
D
C
B
A
E
XCage·8CF3CO2
b)
11.1 Å
12.5 Å
7.0 Å

Figure 1

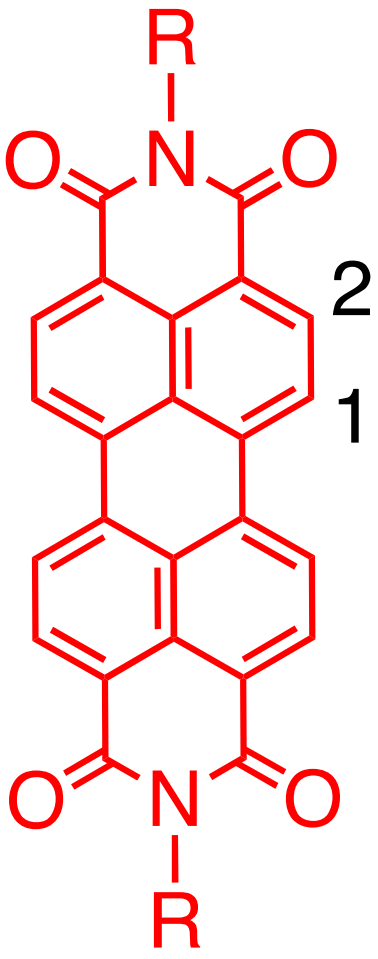

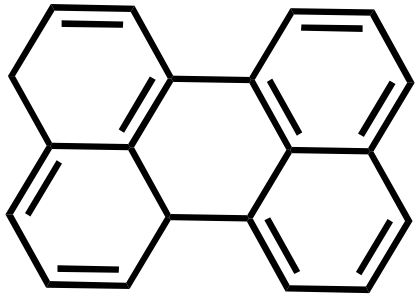

Perylene

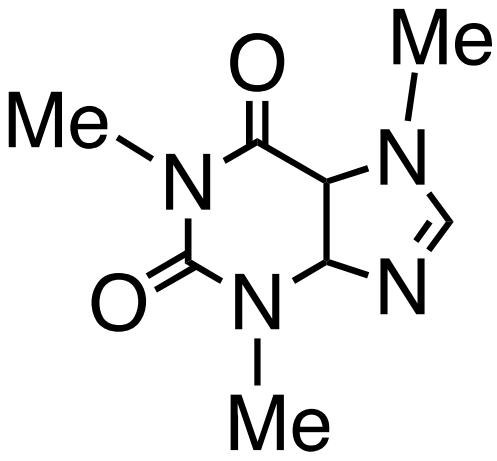

Caffeine

R	
PDI1	$CH_2CH_2NMe_2$
PDI2	$CH_2CH_2[OCH_2CH_2]_{44}OMe$

Figure 2

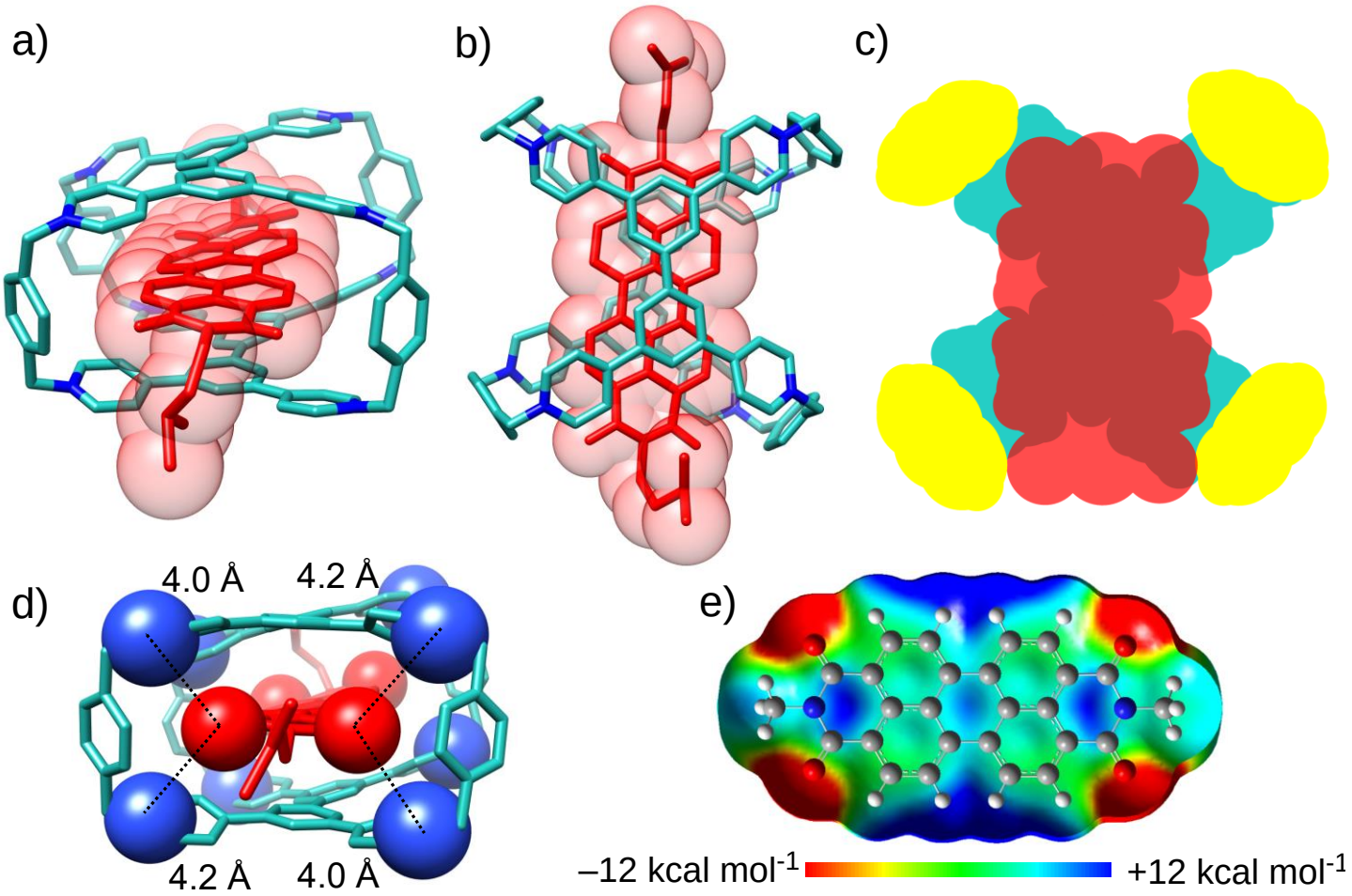

Figure 3

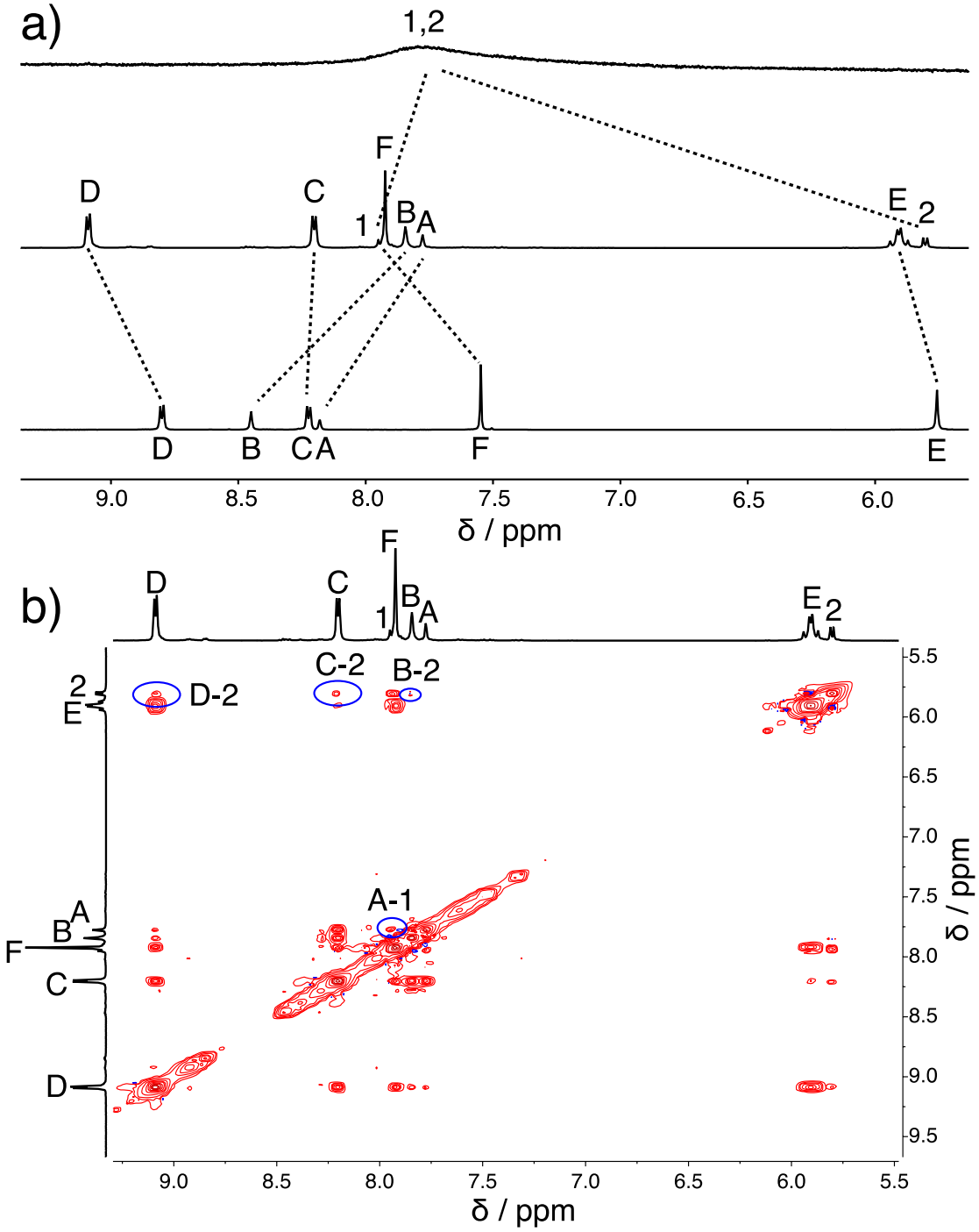
a)
1,2
F
D
C
1
B
A
E
2
D
B
C
A
F
E
9.0
8.5
8.0
7.5
7.0
6.5
6.0
δ / ppm
b)
D
C
F
1
B
A
E
2
C-2
B-2
2
E
D-2
A-1
B
A
F
C
D
5.5
6.0
6.5
7.0
7.5
8.0
8.5
9.0
9.5
δ / ppm
9.0
8.5
8.0
7.5
7.0
6.5
6.0
5.5
δ / ppm

Figure 4

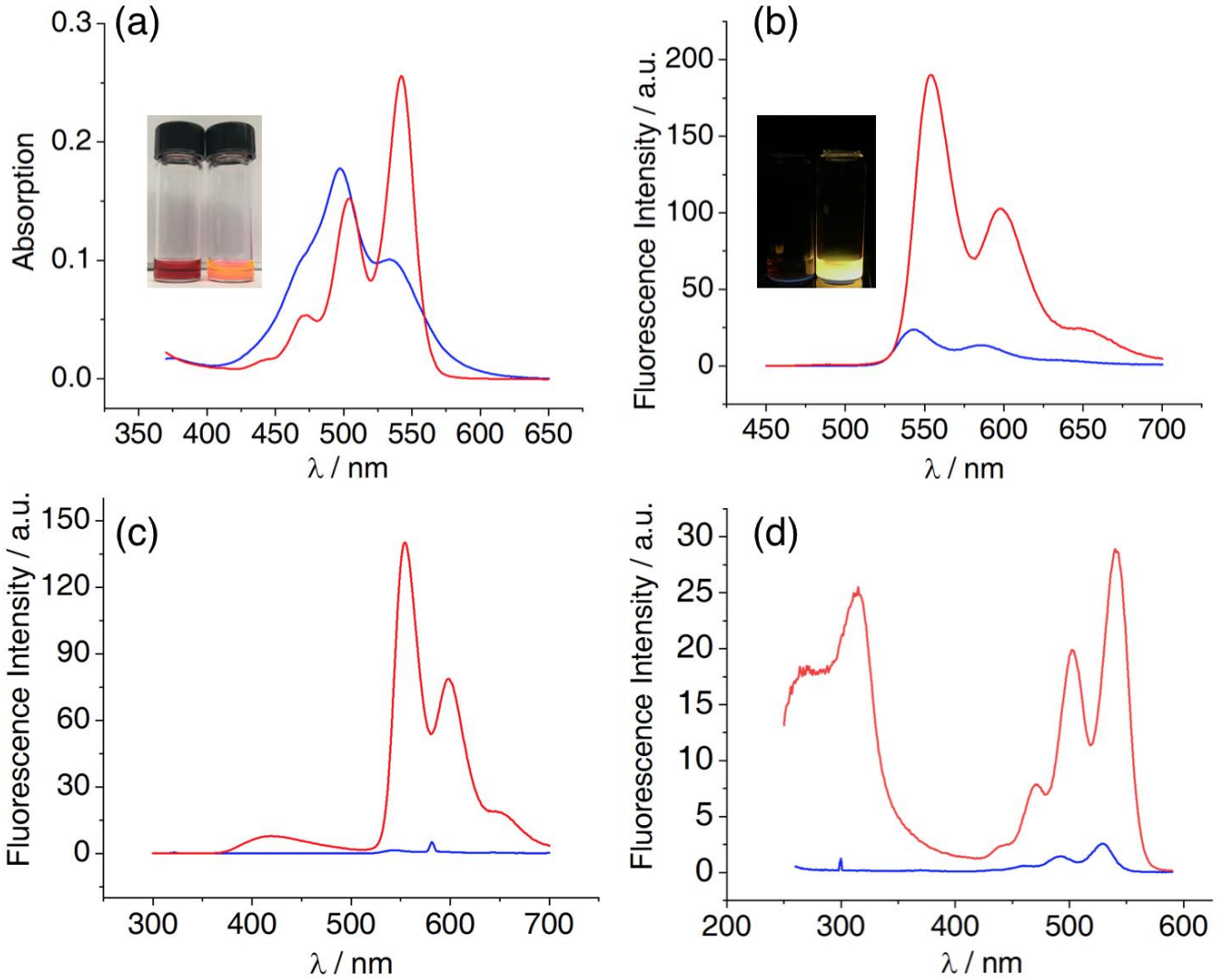
(a)
Absorption
λ / nm
(b)
Fluorescence Intensity / a.u.
λ / nm
(c)
Fluorescence Intensity / a.u.
λ / nm
(d)
Fluorescence Intensity / a.u.
λ / nm

Figure 5

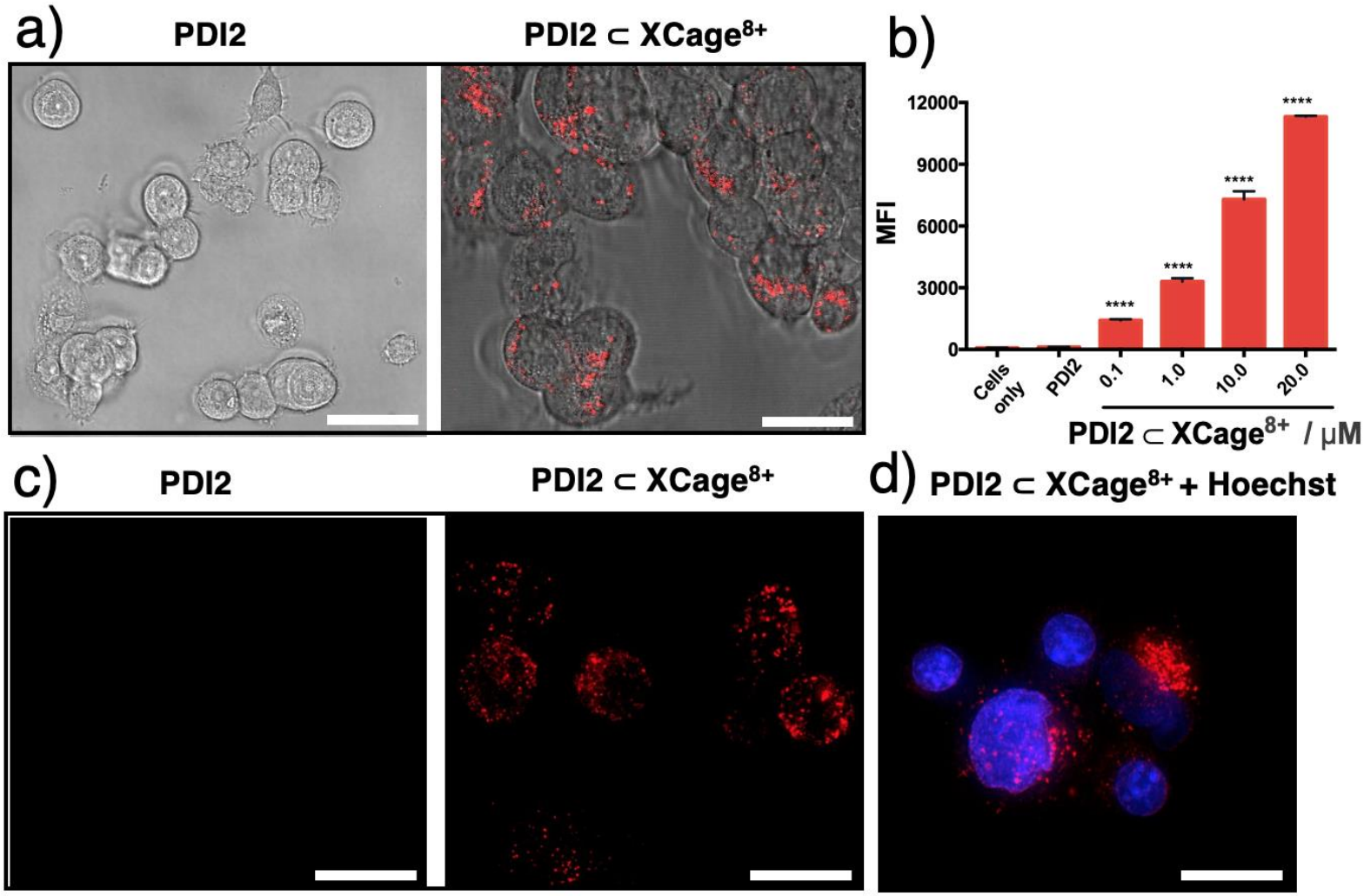
a)
PDI2
PDI2 ⊂ XCage8+
b)
MFI
12000
9000
6000
3000
0
****
****
****
****
Cells only
PDI2
0.1
1.0
10.0
20.0
PDI2 ⊂ XCage8+ / μM
c)
PDI2
PDI2 ⊂ XCage8+
d)
PDI2 ⊂ XCage8+ + Hoechst

Figure 6

Table 1. Binding Constants and Thermodynamic Data at 25 °C[a]

Entry	Solvent	Guest	K_a / M^{-1}		ΔG	ΔH	$T\Delta S$
			Fluorescence	ITC	kcal mol^{-1}		
1	MeCN	Perylene	5.0×10^6	3.6×10^6	–8.9[c]	–6.9	2.0
2	MeCN	PDI2	3.5×10^9	ND[b]	–13.0[d]	–10.2	2.8
3	H_2O	Caffeine	1.2×10^5	1.5×10^5	–7.1[c]	–8.6	-1.5
4	H_2O	PDI2	7.7×10^{10}	ND[b]	–14.8[d]	–14.1	0.7

[a] The standard error is presented in Supporting Information. [b] Not determined. [c] Directly determined by ITC. [d] Estimated from fluorescence titrations

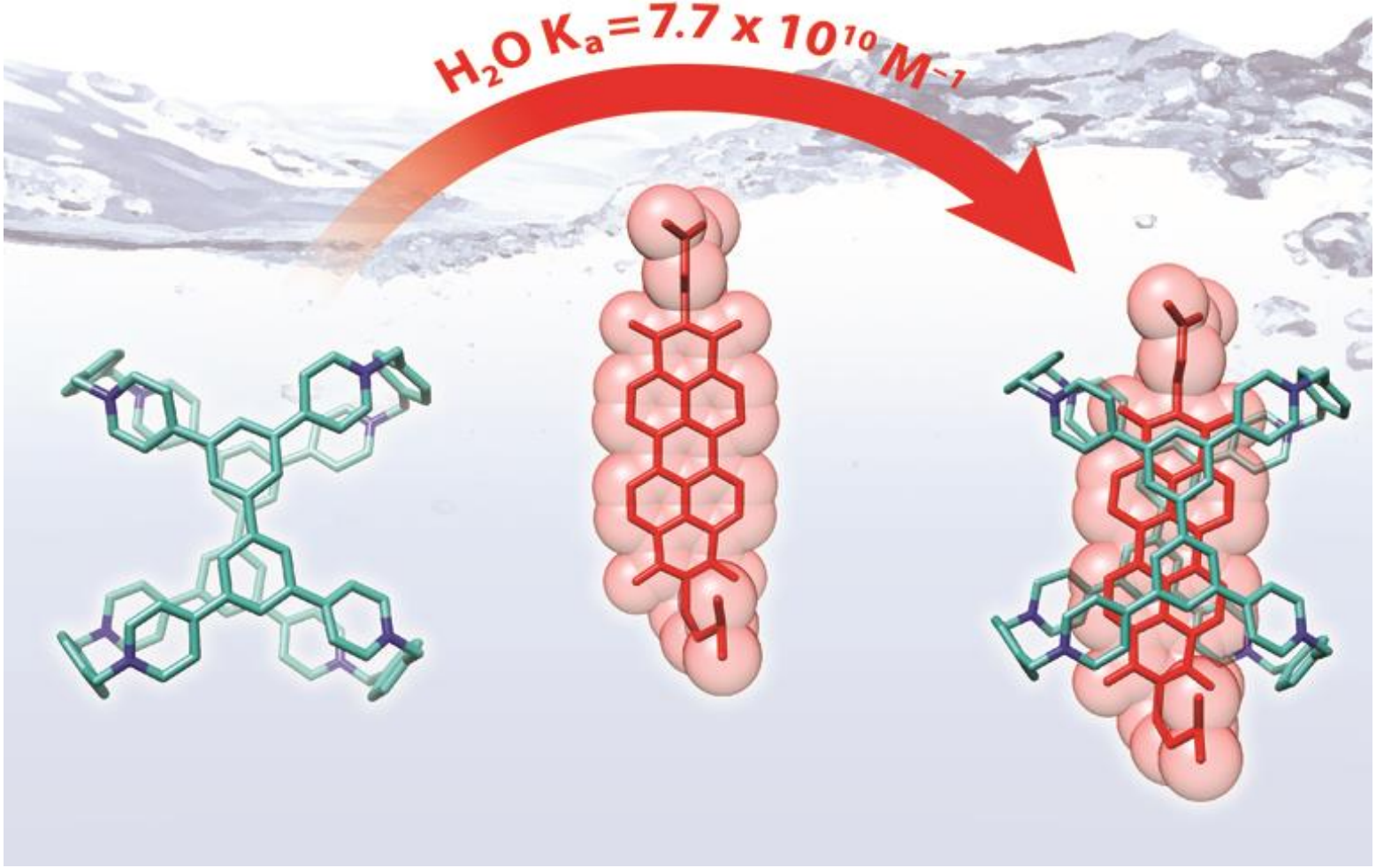

Table of Contents